Microporous and Mesoporous Materials 391 (2025) 113605

Contents lists available at ScienceDirect

Microporous and Mesoporous Materials

journal homepage: www.elsevier.com/locate/micromeso

Hydration pathways of $CaCl_2$ inside matrices with different pore sizes

Michaela C. Eberbach [a,b], A.I. Shkatulov [a,c], H.P. Huinink [a,b,*], H.R. Fischer [d], O.C.G. Adan [a,d]

[a] Eindhoven University of Technology, Den Dolech 2, 5600 MB, Eindhoven, the Netherlands
[b] EIRES, Horsten 1, 5612 AX, Eindhoven, the Netherlands
[c] Iberian Center for Research in Energy Storage, CIIAE, Polígono 13, Parcela 31, "El Cuartillo", 10004, Cáceres, Spain
[d] TNO Materials Solutions, High Tech Campus 25, 5656 AE, Eindhoven, the Netherlands

ABSTRACT

For use as a heat storage material, $CaCl_2$ is often impregnated into porous materials. This is done to stabilize the salt against conglomeration and its dissolution due to the low deliquescence relative humidity. However, $CaCl_2$ has overlapping temperature and water vapor pressure conditions for its trito- and monohydrate, which are kinetically hindered against each other creating path-dependent (de-)hydration steps. These pathways may change under the influence of confinement. These changes can influence the temperature output for heat batteries using $CaCl_2$ composites and could make the taken pathways for hydration and dehydration either more complex or simpler than the pure salt. So, in this research, the hydration and dehydration steps of $CaCl_2$ inside different clays (Vermiculite, Halloysite, and Sepiolite) and silica gels were investigated with respect to their transformations compared to the bulk salt. Therefore, the kinetic phase transition onsets were determined with isobaric TGA measurements together with PXRD in situ experiments to confirm or identify the crystalline phases. This showed that inside pores, $CaCl_2$ forms the monohydrate rather than the tritohydrate. The decrease of pore diameter leads to easier formation of monohydrate over tritohydrate. This trend can be explained by the crystal structures of the hydrates and their unit cell volumes considering that larger crystals are difficult to form in the limited space inside the pore systems. This change in phase transition steps influences the transition temperatures, which affects its application for heat storage.

1. Introduction

In the era of climate change [1–3] and amidst an energy crisis [4], energy storage systems will play a crucial role in mitigating greenhouse gas emissions. One effective strategy involves storing energy in batteries during periods of abundant and affordable supply and releasing it during times of scarcity or higher costs. Various battery types, including electrical and heat batteries, contribute to this effort. Among heat batteries, thermochemical energy storage (TCES) stands out, offering a solution for long-term heat storage [5].

Thermochemical materials (TCMs) are classified as either adsorption materials, such as porous materials, or materials undergoing chemical reactions, such as salt hydrates. Hydrophilic porous materials can adsorb vapor onto their large surface area and generally remain stable over multiple desorption and adsorption cycles, also known as charging and discharging [6,7]. In contrast, salt hydrates undergo a solid-solid phase transition, incorporating vapor molecules into their crystalline structure [8,9]. This reaction between the salt and vapor is exothermic, releasing typically 1–3 GJ/m^3 [10–14]. It can be described by the following equation:

$$MX_i \bullet a\, H_2O_{(s)} + (b-a) \bullet H_2O_{(g)} \leftrightarrow MX_i \bullet bH_2O_{(s)} + \Delta h$$

The two different materials - porous media and salt hydrates - can also be combined by impregnating the salt into the pore system of the porous matrix. This is then called a composite of salt in a porous matrix (CSPM) [15].

Favorable materials to use for low-temperature TCES systems are salt hydrates, because of their high energy storage capacity and ability to store that thermal energy loss-free [16]. Different salts can deliver different temperature outputs and have different energy densities [9]. Examples of these different properties compiled by Donkers et al. [9] are given in Table 1. However, aside from the wanted conditions, the availability and costs of the salt hydrates are important factors among others in deciding which salt is the best fit for a certain application such as domestic heating. $CaCl_2$ is a salt available in large quantities [17–19] and cheap [20–25] because it is a waste product in industrial processes and can be made from limestone or extracted from brine [18,26]. Furthermore, compared to other salt hydrates [20,27], this salt demonstrates high thermal and chemical stability [19,20,28]. Besides anhydrous form, $CaCl_2$ has multiple known hydrates [29–33]: anhydrate (0 mol H_2O/mol $CaCl_2$), tritohydrate (1/3} H_2O/mol $CaCl_2$), monohydrate (1H_2O/mol $CaCl_2$), dihydrate (2H_2O/mol $CaCl_2$), α-, β- and

* Corresponding author. Eindhoven University of Technology, Den Dolech 2, 5600 MB, Eindhoven, the Netherlands
E-mail address: h.p.huinink@tue.nl (H.P. Huinink).

https://doi.org/10.1016/j.micromeso.2025.113605
Received 13 December 2024; Received in revised form 17 February 2025; Accepted 18 March 2025
Available online 19 March 2025
1387-1811/

Table 1
The hydration and dehydration temperatures ($T_{hydration}$ at 12 mbar water vapor pressure and $T_{dehydration}$ at 20 mbar water vapor pressure), along with the energy densities, of various salt hydrates are provided in the following examples, adapted from Donkers et al. [9].

Salt	Higher hydrate	Lower hydrate	Energy density open system [GJ/m^3]	$T_{hydration}$ [°C]	$T_{dehydration}$ [°C]
$Al_2(SO_4)_3$	6	0	3.19	293	306
$Ba(OH)_2$	8	3	1.91	43	49
$CaSO_4$	2	0	1.29	20	26
K_2CO_3	1.5	0	1.30	59	65
LiBr	1	0	1.77–2.01	94–103	101–110
LiCl	1	0	1.83–2.08	66–73	72–80
$MgBr_2$	6	0	3.02	135	144
$MgCl_2$	2	0	2.23	118	214

γ-polymorphs of the tetrahydrate ($4H_2O$/mol $CaCl_2$) and hexahydrate ($6H_2O$/mol $CaCl_2$). Therefore, it was used in many studies for heat storage, also in combination with other salts [34–36] and impregnated into porous materials [37–39]. The impregnations were done mainly due to the low deliquescence relative humidity (DRH), which makes the salt difficult to handle in the pure form [40,41]. Additionally, the impregnation improves the heat and mass transfer through the material and provides the possibility to take advantage of the deliquescence phase transition [42].

The hydration pathways of $CaCl_2$ are not well understood, as evidenced by the discovery of the tritohydrate by Sinke et al. [32] and subsequent investigations conducted by Molenda et al. [33]. Molenda's research revealed distinctions between the hydration and dehydration pathways at water vapor pressures below 100 mbar [33]. Notably, during hydration from the anhydrate to the dihydrate, only one intermediate step, the tritohydrate, was identified through thermogravimetric analysis (TGA) measurements and in-situ powder X-ray diffraction (PXRD) experiments [43]. Surprisingly, no monohydrate was observed during hydration. Conversely, during dehydration, only the monohydrate was present below 100 mbar water vapor pressure, with no indication of the tritohydrate detected using TGA or PXRD methods [43]. Furthermore, recent determinations of the crystal structures of the trito- and monohydrate [43] provide insights that can help explain the kinetic hindrance of the monohydrate formation during hydration and the tritohydrate formation during dehydration, leading to these path-dependent steps.

This kinetic hindrance between the transitions of the hydrates gives rise to the opportunity for the behavior of the salt hydrate to change inside porous matrices. Many different combinations of $CaCl_2$ with porous matrices were tested in the literature [14,44,45]. Aristov et al. tested $CaCl_2$ inside two pore sizes of silica gels [46] and inside vermiculite [47]. Through the calculations of the loading [mol H_2O/mol $CaCl_2$], the hydrate steps in silica gels were identified as the anhydrate and dihydrate, while path-dependent behavior with trito- and monohydrate is assumed for the vermiculite composites. Additionally, XRD and ^{2}H NMR studies were performed by Gordeeva et al. [48] which show that in these pores no crystalline salt or its hydrates can be detected by XRD but the NMR study show the formation and melting of the hydrates. However, no comparison of the kinetic regimes of hydration-dehydration in different matrices and the possible reasons for the different pathways was found in the literature.

Many other porous materials were tested as matrices for the $CaCl_2$ salt. Examples of this are in the works of Jabbari-Hichri et al. [49] where silica-gel, alumina, and bentonite as matrices were tested, or Casey et al. [50] where activated carbon and zeolite 13X were examined. Other studies also include salt mixtures stabilized inside porous systems, like in the work of Zhang et al. [51] where a mixture of $MgSO_4$ and $CaCl_2$ was impregnated into vermiculite.

Except for Aristov et al.'s works [46,47], most studies on $CaCl_2$ composites neglect the intermediate hydration steps, focusing instead on application properties [39,42,50,52–54]. Hence, to get a deeper insight into which (de-)hydration steps are performed by the $CaCl_2$ as a path-dependent salt hydrate in different matrices and different pore sizes complementary measurement techniques should be used to ensure weight changes are correlated to the crystalline phases formed. This research aims to shed light on it and to provide an explanation of why these steps deviate from those observed in the pure salt, ultimately providing a more thorough understanding of the expected temperature and energy outputs from a $CaCl_2$ composite in a heat battery.

In this study, the salt hydrate was impregnated into clays, namely Vermiculite, Halloysite, and Sepiolite. These matrices were chosen due to their availability and low price, which makes them favorable to use as TCES materials. Likewise, they provide a large range in pore sizes from macropores for Vermiculite over mesopores in the Halloysite to a combination of mesopores and micropores in the Sepiolite. Additionally, reference composites were made using silica gels with varying pore diameters ranging from 2 to 11 nm, similar to the ones used in Ref. [55]. These silica gels were used for the reference composites because they are well-understood systems and can provide different average pore sizes with the same pore wall composition.

List of abbreviations

DRH	Deliquescence Relative Humidity
DVS	Dynamic Vapor Sorption
MSZ	Meta-Stable Zone
PXRD	Powder X-Ray Diffraction
RH	Relative Humidity
TCES	Thermo-Chemical Energy Storage
TCM	Thermo-Chemical Material
TGA	Thermo-Gravimetric Analysis
SI	Supplementary Information
$CaCl_2$	Calcium(II) chloride or Calcium dichloride
VCC	composite of Vermiculite + $CaCl_2$
HCC	composite of Halloysite + $CaCl_2$
SCC	composite of Sepiolite + $CaCl_2$
SGxCC	composite of Silica gel with average x nm pores + $CaCl_2$

2. Materials and methods

2.1. Materials

2.1.1. Synthesis of the composites

Calcium dichloride ($CaCl_2$) was ordered from Sigma-Aldrich in the form of the dihydrate $CaCl_2 \cdot 2H_2O$, ACS reagent, ≥99.0 %). For the use as a TGA sample, the salts were ground very lightly in an agate mortar preheated in a 160 °C oven, because of the deliquescence of the salts, before they were used in measurements.

As matrices for the composites, mesoporous, amorphous silica gels (SGs) with different pore diameters and the clays Halloysite, Sepiolite, and Vermiculite were used. The average pore sizes of all the used matrices are given in Table 2. The SG4 was ordered from Fisher Scientific, while all other SGs were ordered from Sigma-Aldrich, and all of them were used without any pre-treatment. The Halloysite (Halloy or H) was purchased from Sigma-Aldrich, while the Sepiolite (Sepio or S) was supplied by Tolsa Spain as Pangel S9. The Vermiculite (V) was purchased from Karopack. The clays were not modified before their use as pure matrix since they were already in a purified and powdered form.

The composites were synthesized using two different methods: the dry incipient and a freeze-drying method. The dry incipient method was not possible with the Halloysite and Sepiolite used in this study, because the resulting mixtures would not resemble powder anymore, and were all clung together in a block even without the use of salt, but only H_2O. The silica gel composites were prepared through the dry incipient method [46,56–59], while clay composites were obtained using a

Table 2
An overview of the composites is given with the components used to make the composites as the used matrix with $CaCl_2$. Additionally, the abbreviation for each composite, the abbreviation for the composite, the average pore diameter of the used matrix, the salt content (ϕ), and the weight ratio between the salt and matrix. A saturated solution of $CaCl_2$ was used to calculate the ϕ and the ratio between the two components. Here, m stands for mass in [g].

Composite	Abbreviation	pore d_{avg} [nm]	ϕ [wt %]	m_{salt}/m_{matrix} [g/g]	Supplier
Vermiculite + $CaCl_2$	VCC	>200	72.9	2.69	Karopack
Halloysite + $CaCl_2$	HCC	15	48.3	0.93	Sigma-Aldrich
Sepiolite + $CaCl_2$	SCC	8	49.3	0.86	Tolsa Spain
Silica gel (11 nm) + $CaCl_2$	SG11CC	11	38.9	0.64	Sigma-Aldrich
Silica gel (6 nm) + $CaCl_2$	SG6CC	6	30.7	0.44	Sigma-Aldrich
Silica gel (5 nm) + $CaCl_2$	SG5CC	5.8	31.6	0.46	Sigma-Aldrich
Silica gel (4 nm) + $CaCl_2$	SG4CC	3.8	22.2	0.29	Fisher Scientific
Silica gel (3 nm) + $CaCl_2$	SG3CC	3.3	15.9	0.19	Sigma-Aldrich
Silica gel (2 nm) + $CaCl_2$	SG2CC	2.5	16.12	0.19	Sigma-Aldrich

freeze-drying method. For vermiculite composites, a vacuum variation of the dry incipient method was employed to ensure the removal of air pockets in the pore system. The composites, along with their abbreviations (''V'' for Vermiculite, ''H'' for Halloysite, ''S'' for Sepiolite, and ''SGx'' for silica gels with an average pore diameter denoted as "d_{avg}" in nanometers), are listed in Table 2.

The process of the dry incipient method, illustrated in Fig. 1a), involved drying matrices in an oven at 160 °C overnight to determine their dry weight. Subsequently, dried silica gels were mixed with a saturated aqueous salt solution where the volume filled exactly the accessible pore volumes.

The two components were mixed until resembling a dry powder due to the solution being adsorbed into the pores through capillary forces. This mixture was then dried overnight in an oven at 160 °C. In contrast, for vermiculite composites, the clay matrix and $CaCl_2$ were mixed under vacuum instead of ambient conditions.

The synthesis of clay composites as depicted in Fig. 1b) was done by first drying the matrix in an oven at 160 °C to determine the weight of the pure matrix. Next, the matrix was put into a suspension with demineralized water. The saturated solution of the salt was added in a certain ratio to the matrix in the suspension (1 mL saturated solution per gram of matrix). The suspension was thoroughly mixed and then freeze-dried to obtain a dry powder of the composite.

Through weighting the samples at various steps in the procedures or calculations with the salt concentration in the saturated solution and the used amount of solution per weight of the matrix, the masses (m) of the two components, the salt content (ϕ) and different ratios could be determined as shown in Table 2. Here, the ϕ was calculated as:

$$\varphi = \frac{m_{salt}}{m_{salt} + m_{matrix}} \bullet 100\% = \frac{m_{salt}}{m_{composite}} \bullet 100\%$$

2.2. Pore volume, pore size and pore size distribution

The pore structure of the matrices was investigated by N_2 adsorption and desorption at 77K together in a Micromeritics Gemini VII. First, the samples were prepared by degassing them in the preparation station at 150 °C with N_2 flow overnight (16 h). The measurement was done as isothermal adsorption and desorption at 77 K with pressures from the lowest vacuum as the starting reference point to 0.998 p/p^0. By doing so, the average pore diameter, surface area, and accessible pore volume could be calculated. The BJH method [60] was used to calculate the average pore diameter from the whole desorption range and determine the accessible pore volume and the BET theory [61] to determine the surface area in m^2 per g of sample from the data points between 0.01 and 0.3 p/p^0.

The composites were also subjected to these measurements to find the position of the salt inside or around the porous matrices.

2.3. Isobaric TGA cycles

Isobaric water sorption and desorption of the pure salts and the composites were investigated using Thermo-Gravimetric Analysis on two TGA devices, i.e. Mettler Toledo TGA/SDTA851e and Mettler Toledo TGA/DSC 3+, similar to the measurements described in Ref. [55]. The two TGA setups from Mettler Toledo were used together with a home-build or a Cellkraft humidifier. The oven temperature could be controlled between 25 and 1000 °C and this temperature was recorded together with the sample temperature. The sample was located in both devices on a balance arm inside the oven with an accuracy of ±1 μg.

Both machines had an inlet for gas flows connected to one of the humidifiers. The home-build humidifier operated at 18 °C and mixed a dry (0 % RH) and a wet (100 % RH) N_2 flow to generate a water vapor pressure between 0 and 20 mbar. This was done by Arduino-controlled flow meters, which could mix the two flows in different ratios to create the desired water vapor pressure. This home-build device was connected to the TGA/SDTA851e. The second humidifier was a Cellkraft Humidifier P-2 operating at 25 °C, which worked via a feedback loop from an RH sensor at the outlet of the humidifier and was connected to the TGA/DSC 3+. Both devices had a 300 mL/min flow rate over the sample inside the TGAs.

The temperatures of both TGA's were calibrated to an accuracy of

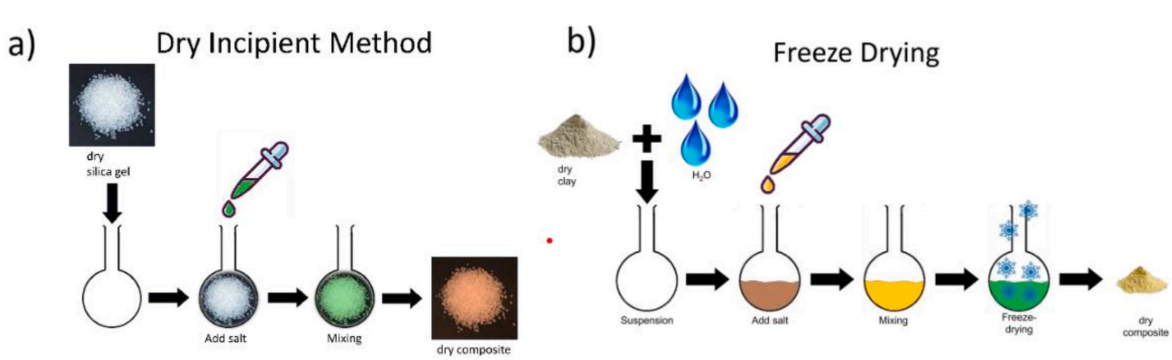

Fig. 1. The schematic representation of the composite synthesis using a) the dry incipient method for the silica gels and b) the freeze-drying method for the clay minerals.

0.2 K using the melting points of benzophenone, indium, and zinc, which give a differential signal during this endothermic process [62], while the humidifiers were calibrated to an accuracy of ±1 mbar using the gravimetric signal at the deliquescence points of $LiCl·H_2O$, CH_3COOK, $K_2CO_3·1.5H_2O$, $MgCl_2·6H_2O$ and $Mg(NO_3)_2·6H_2O$ at 25 °C and a validity check at higher temperatures (45 and 60 °C) using $LiCl·H_2O$ [63].

A temperature program was run with a sample while the humidifier was turned on simultaneously at the desired water vapor pressure. Thereby, the program was usually structured to contain an isothermal step at a high temperature to ensure complete dehydration, then cooling at a certain K/min rate, an isothermal step at the lowest temperature to ensure full hydration, and then heating at the same rate as the cooling back to the high temperature, which was again held in an isothermal step to ensure full dehydration again. The resulting weight changes were used to calculate a parameter called loading (L), which describes the weight change of the sample in [mol H_2O per mol salt]. The loading was calculated similarly to Ref. [64] using the dry weight at high temperatures of each sample and the current weight together in:

$$L = \frac{m - m_d}{M_w} \bullet \frac{M_{salt}}{\varphi \bullet m_d}$$

At this moment, m [g] stands for the current mass of the sample, m_d [g] for the dry sample mass, M_w [g/mol] for the molecular mass of water (18.015 g/mol), and M_{salt} [g/mol] for the molecular mass of the salt, either calcium(II) dibromide anhydrate (199.89 g/mol) or calcium(II) dichloride anhydrate (110.98 g/mol). Lastly, ϕ represents the weight content of the salt in the sample, which is between 0 and 100\% for the composites and equal to 100 % for the pure salt samples.

With these measurements, the temperatures at which the phase transitions start can be determined [65]. These onsets are observed at the beginning of the weight change, following a horizontal plateau of the starting hydrate.

2.4. *Isobaric Powder-XRD in-situ*

X-ray diffraction was performed as described in Ref. [55] by using a Rigaku MiniFlex diffractometer in continuous scan mode with a divergent slit of 0.625° and a D/teX Ultra2 detector, using Cu K_α-radiation and K_β filter. To identify the crystalline phases of the confined salt hydrates and to observe the phase transitions, Powder X-ray diffraction (PXRD) in situ was performed using a high-temperature attachment, called Anton Paar BTS 500 heating stage. Additionally, the built-in diffractometer and an attached humidifier, which can create flow of nitrogen with 0–20 mbar water vapor over the sample, were used in the measurements. The measurements were carried out with Bragg-Brentano geometry at 2θ = 5–75° with step sizes between 0.005 and 0.01° and speed of 1–10°/min. The humidifier worked similarly to the home-build humidifier of the TGAs, but the flow rate was set to 800 mL/min, because of larger sample sizes.

Two types of measurements were performed with the PXRD. First, a detailed scan of each dry sample, salts, and composites, was performed. This was done at 150 °C and 0 mbar of water vapor partial pressure with the 2θ ranging from 10 to 75°, a step size of 0.005° and a speed of 3°/min. Each of these scans took around 25 min next to the temperature being held constant for some time to ensure complete dehydration for the anhydrate sample.

Secondly, isobaric in-situ measurements were performed using several scans at different temperatures with a constant p_{vap} = 12 mbar turned on. Since the in-situ measurements needed several scans (30–50), the scans were shortened to reduce the measurement time. Considering that the strongest reflections of the anhydrate and different hydrates lie between 10° and 50°, the range of 2θ was shortened from 10 - 75° to 10–50° with a step size of 0.050° and a speed of 5°/min, which changed the recording time of one scan to 9 min.

The isobaric PXRD in-situ measurements for the $CaCl_2$ samples were executed in the following way. First, the sample was brought to a starting temperature of 150 °C when the first scan was recorded. Then, the temperature was decreased from 104 °C to 60 °C, in steps of 2K. A diffractogram was recorded at each temperature step. Then the diffractogram at the lowest temperature of 45 °C was measured with a subsequent increase in temperature from 84 °C to 130 °C in steps of 2K and end temperature 150 °C. The start, lowest, and end temperatures were held for 3 h before the reflections were recorded to ensure that the sample was completely transitioned. In contrast, all other temperatures were only held for either 1 or 30 min before recording the reflections, for an experiment similar to the TGA measurements or slow measurements to get clearer patterns of the intermediate phases.

3. Results and discussion

3.1. *The (de-)hydration paths of the clay composites*

As described in the literature, $CaCl_2$ has complex hydration and dehydration steps [33,43]. Therefore, the steps taken in the tested clay-$CaCl_2$ composites were examined to evaluate the temperatures at which the salt inside the pore structures hydrates and dehydrates. Starting with the composite of vermiculite and $CaCl_2$ (VCC), isobaric TGA measurements were performed. One example at 12 mbar is shown in Fig. 2. Here, the temperatures at which the phase transitions start are labelled with the letters A to F.

The loading [mol H_2O/mol $CaCl_2$] reveals a pattern closely resembling that observed in the bulk salt [43]: 0–1/3-2-1-0. During the transition from the anhydrate to the tritohydrate (onset A) and from the tritohydrate to the dihydrate (onset C) in the hydration process, there are subtle intermediate steps (onsets B and D) that were not evident in bulk $CaCl_2$.

To compare the crystalline phases in the VCC with those in bulk salt, an isobaric in situ PXRD measurement was conducted. The results showed that the same hydration and dehydration steps observed in pure $CaCl_2$ also occurred in this analysis, as detailed in the Supporting Information (SI). However, while TGA measurements indicated smaller onset steps (B and D) during hydration, no additional transitions or secondary phases were detected in the in situ PXRD measurements. This discrepancy may be due to the minor size of these additional phase transitions relative to the dominant steps (0–1/3–2; A and C). This explanation is supported by the minimal loading changes observed in the TGA measurements for steps B and D, suggesting that the quantity of the additional phase was too low to be detected in the in situ PXRD

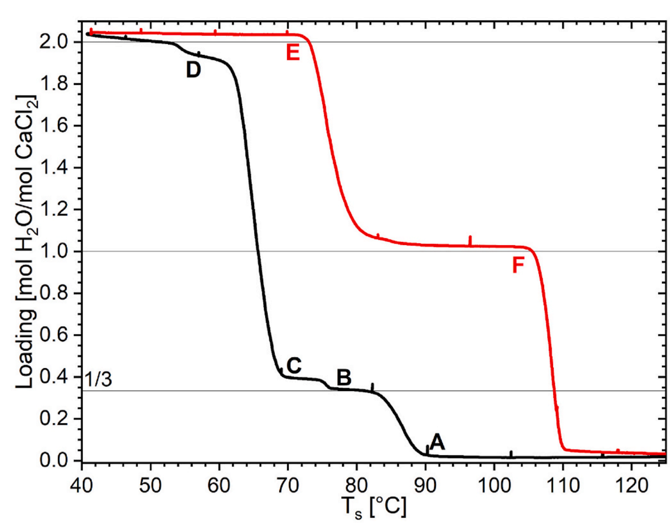

Fig. 2. Isobaric TGA measurement of the Vermiculite + $CaCl_2$ composite at 12 mbar and a heating/cooling rate of 0.1 K/min with the hydration during cooling in black and the dehydration during heating in red.

measurements.

Comparing the kinetic onsets found in the TGA measurement from the composite with the \hl{kinetic} phase transition onsets of the pure salt in Ref. [43], showed that the transition of 0–1/3 (A), 1/3-2 (C), 2-1 (E) and 1-0 (F) from the composite were coinciding with the same ones of the pure salt. Additionally, the onset during hydration denoted as D in Fig. 2 correlated well with the 1–2 onset of $CaCl_2^{43}$ in the sense that at the same water vapor pressure the onset temperatures are similar. Thus, it is assumed that the additional phase transitions (B and D) result from the 0-1-2 steps occurring in a minor portion of $CaCl_2$ within the porous system, while the major part of $CaCl_2$ follows the 0–1/3-2 steps. These comparisons at 12 mbar are presented in Table 3.

These results from the VCC composite being similar to the bulk $CaCl_2$ salt are as expected since the large pores (>1000 nm) of the vermiculite should exert little influence on the salt crystals. The large pores give the salt space to form larger crystals and so the salt acts like the unhindered bulk salt.

Next, the composite of Halloysite and $CaCl_2$ was examined. The N_2 isotherms of the composite showed a significant decrease of the pore volume corresponding to 0.6 g of salt per g of Halloysite indicating that the majority of the salt is distributed inside the pore system. Additionally, the composite was investigated with EDX which should no bulky $CaCl_2$ crystallines were found on the surface of the clay. These results are shown in the SI. The isobaric TGA measurement of this composite at 12 mbar is shown in Fig. 3a) as the red line. Like with the VCC and the pure salt, the dehydration showed the 2-1-0 kinetic steps. However, during the hydration, four onsets were observed. However, unlike for the VCC, the change in loading was roughly similar between the onsets instead of one major set and one minor one. Because no stable plateaus in loading were formed, the phases could not be identified by the loading.

Hence, to identify the crystalline phases during hydration, isobaric PXRD in situ was used again. During the hydration process, identifying the precise kinetic onsets of phase transitions posed a challenge. Nevertheless, distinct reflections from both the tritohydrate and monohydrate were detected. An illustrative example of this phenomenon is presented in Fig. 4a). In the figure, the reflections from the tritohydrate (highlighted in blue) are prominently visible, particularly around 31.5° and 33° for 2θ. Although the monohydrate's visibility is reduced due to its later formation during the measurement, it can still be identified by the reflection (highlighted in red), notably around 15° for 2θ. It's worth noting that reflections not highlighted either originate from the Halloysite clay, as indicated in the SI or possess insufficient intensity for reliable identification. Furthermore, reflections from the dihydrate might already be visible, like indicated by the reflections around 14.5° for 2θ. This is the result of the different transition temperatures towards and from the trito- and monohydrate. For the dehydration, it was as clear as during the TGA measurement that the HCC was performing the 2-1-0 steps.

Similarly to the hydration onsets of VCC, the onsets of HCC were compared to the onsets of the pure salt determined in Ref. [43]. Here, it was found again that the three onsets A, C, and D in Fig. 3a) overlap with the 0–1/3, 1/3-2 and 1–2 of the pure salt. The fourth onset, labelled B, was close to VCC's suspected 0–1 onset. Like it was suspected for the VCC, the HCC is likely also having two parts of the impregnated salt: one hydrating via 0–1/3-2 and the other via 0-1-2. However, unlike in the VCC, the two parts are more similar in the amount of salt, at least no majority or minority part can be identified. This is supported by the PXRD findings with both trito- and monohydrate unlike with the VCC composite, which did not show identifiable reflections for the monohydrate.

This change in hydration behavior of the HCC composite compared to the VCC could be explained by the smaller pore size in the Halloysite. The Halloysite used in this study consists of tubes with an average pore size of 15 nm, which was determined by isotherm N_2 adsorption and desorption measurements and BJH analysis [60]. The N_2 isotherm is given in the SI. This pore size is far smaller than the pore sizes of the Vermiculite, which were too large to analyze with the N_2 method. Hence, it can be assumed that the influence of the confinement and/or the interaction with the pore wall interface is stronger on the $CaCl_2$ in this composite than in VCC. However, also the compositions of the pore walls differ between the two clays. This could cause different interactions with the salt hydrate, for example through epitaxial growth.

As the last clay composite, the composite of Sepiolite and $CaCl_2$, SCC, will be discussed. Like with the HCC, the N_2 isotherms of the composite showed a significant decrease of the pore volume corresponding to 1.4 g of salt per g of Sepiolite indicating that the majority of the salt is distributed inside the pore system combined with blocking of pores from the salt. Additionally, the composite was investigated with EDX which should no bulky $CaCl_2$ crystallines were found on the surface of the clay. These results are shown in the SI. Furthermore, the TGA and XRD results show no indications of the bulk salt behavior, showing that only an insignificant amount of salt can be on the outside of the matrix. The kinetic steps during the 12 mbar isobaric TGA measurement are shown in Fig. 3a) as the blue line. Here, only two onsets are distinguishable during the hydration and also during the dehydration. The dehydration, with steps 2-1-0, is the same as for the bulk salt [33,43] and as earlier described for the other two clay composites VCC and HCC. The hydration instead is different from all three of these systems by following the steps 0-1-2 instead of 0–1/3-2 or variations with both intermediates. The loading [mol H_2O/mol $CaCl_2$] of the different steps are not exactly 1 mol/mol or 2 mol/mol due to the adsorption of the Sepiolite matrix. Thus, PXRD in situ was used again to explore which hydrated phases were formed. The PXRD results clearly show the monohydrate as the intermediate step between the anhydrate and dihydrate both during hydration and dehydration as depicted in Fig. 4b). Again, the reflections of the monohydrate are highlighted in red, and reflections of the clay matrix Sepiolite are visible beside the $CaCl_2$ ones, which are given in the SI with the PXRD diffractograms of the other clay matrices.

The onset temperatures of the SCC composite were compared to the ones of the pure $CaCl_2$ like it was done for the other two clay composites in Table 3. This showed that the dehydration onsets correlate well with the 2-1 and 1-0 onsets of the bulk salt and the other composite. Additionally, the 1–2 hydration onset was in the same temperature range as the pure salt hydrate and the other two clay composites. The unchanged phase transition onsets of the composites compared to the bulk salt correlates well with earlier works [55], where it was shown that the pore size has little effect on these onsets. The 0–1 hydration onset was close to the 2-1 dehydration and thus also correlated well with the earlier results. So, while the hydration steps that are taken differ between the composites and with the salt, but the onsets for the same hydration transitions seem not to be affected by the matrix or the pore size in this work. Additionally, no change to the 2θ position of the reflections could be detected, thus the crystalline phases did not experience changes to their lattice structure such as ion exchange or solid solutions.

Table 3
The onset temperatures of hydration and dehydration at 12 mbar water vapor pressure of the tested composites in comparison to the pure $CaCl_2$.

Phase transition	$CaCl_2$ [°C]	VCC [°C]	HCC [°C]	SCC [°C]	SG11CC [°C]	SG6CC [°C]
0–2	–	–	–	–	75	85
0-1/3	89	90	85	–	–	–
0–1	–	76	76	74	–	–
1/3-2	69	70	68	–	–	–
1–2	59	56	57	60	55	–
2–0	–	–	–	–	85	90
2–1	78	72	81	74	–	–
1–0	110	105	111	107	108	–

3.2. Silica gel composites as reference samples

As was shown, the clay composites had different hydration pathways

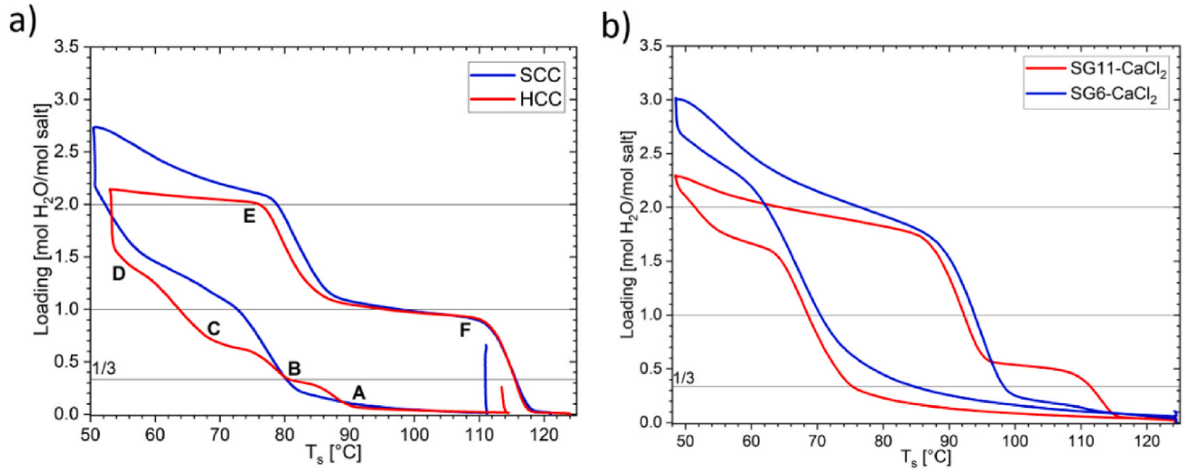

Fig. 3. The results from isobaric TGA cycling at 12 mbar from a) the clay composites with red for the Halloysite and blue for the Sepiolite composite, b) the silica gels (SGs) composites with red for the 11 nm average pore diameter and blue for the 6 nm one.

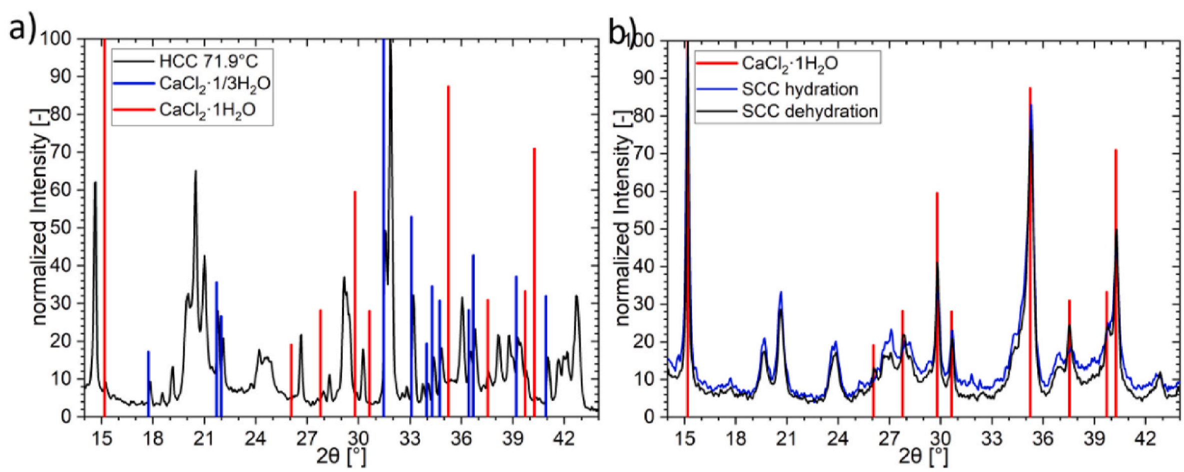

Fig. 4. The results from isobaric PXRD in-situ at 12 mbar from a) HCC hydration (black curve), and b) SCC hydration (blue curve) and dehydration (black curve) in comparison with the reflection positions of the pure bulk $CaCl_2$ from Ref. [43] as the blue vertical lines for the tritohydrate and the red vertical lines for the monohydrate.

from each other, but also from the bulk salt. This could either come from the difference in pore wall composition in interaction with $CaCl_2$ or due to the difference in pore sizes/diameter. To investigate the second aspect, silica gels with different pore sizes were used as matrices for the salt hydrate like it was done in Ref. [55]. The pore sizes were calculated from N_2 isotherms, which are shown in the SI. Additionally, the isotherms of the silica gel composites, like with the clay composites, showed significant decreases of the pore volumes corresponding to 2.4 and 1.3 g of salt per g of silica gel for the SG11 and SG6 indicating that the majority of the salt is distributed inside the pore system combined with blocking of pores by the salt. Additionally, the composite was investigated with EDX which should no bulky $CaCl_2$ crystallines were found on the surface of the silica gels. These results are shown in the SI. Furthermore, the TGA and XRD results for SG11CC and SG6CC show no indications of the bulk salt behavior, showing that only an insignificant amount of salt can be on the outside of the matrix.

The composites with silica gels (SGs) with average pore sizes smaller than 6 nm did not exhibit any clearly visible kinetic phase transition onsets, which is the result of overlapping hydration and deliquescence like observed for $CuCl_2$ in Ref. [55] with a higher deliquescence relative humidity than $CaCl_2$. Furthermore, in some cases, they experienced issues with pore blockage (see SI). Thus, only the SG6CC and SG11CC composites were further investigated.

Subsequently, the isobaric TGA cycles of the two composites were initially recorded (see Fig. 3b)), with SG6CC represented in blue and SG11CC in red. When looking at the curve of SG6CC, only one kinetic onset for hydration and one for dehydration are observable. This contrasts strongly with observations of clay composites and pure $CaCl_2$, which typically display between two and four onsets for hydration and two for dehydration. Based on the loading [mol H_2O/mol $CaCl_2$], it appears that the salt takes up water directly from the anhydrate to the dihydrate and reverses during dehydration.

In line with the methodology applied to the clay composites, the SG6CC underwent a PXRD in situ measurement to ascertain the crystalline phases formed. The anhydrate observed at the beginning of the measurement and the dihydrate at the end of hydration mirrored those in pure $CaCl_2$, albeit with an amorphous ''peak'' between 15 and 30° of 2θ due to the silica gel. However, the intermediate step identified in multiple consecutive diffractograms was not a singular hydrate phase but rather both the monohydrate and the dihydrate. One such diffractogram displaying this intermediate stage is depicted in Fig. 5, notably marked by the reflection around 14.5° for the dihydrate and 15° for the monohydrate, along with reflections around 32 and 35° for 2θ, indicating the presence of both hydrates in the sample. Conversely, no intermediate step, neither a single hydrate or multiple hydrates, was detected during dehydration, revealing a direct transition from

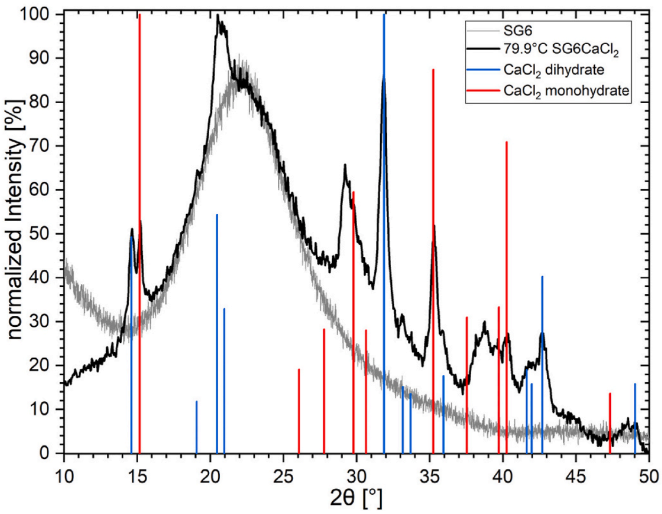

Fig. 5. The results from isobaric PXRD in-situ at 12 mbar from SG6+CaCl2 hydration.

dihydrate to anhydrate (see SI).

Contrary to the anticipated comparison with one of the clay composites i.e. Sepiolite due to its smallest average pore size of 8 nm, the silica gel composite SG6CC displayed a novel (de-)hydration behavior, largely bypassing intermediate steps. This deviation was evident in both TGA and PXRD in situ measurements, except for the occurrence of the monohydrate-dihydrate mixture step during hydration. Comparison of the onsets found for the SG6CC composite with the phase diagram in Ref. [43] revealed that while the hydration onset neighbors the suspected 0–1 onset of the clay composite, the dehydration onset did not correlate with any known onsets.

In the SG11CC composite, similar steps to those observed in SG6CC were evident, as depicted in Fig. 2b). However, there were additional small steps towards the end of hydration and dehydration. The phases were not readily identifiable from the loading data, as the hydration step fell between the mono- and dihydrate, while the dehydration step lay between the mono- and anhydrate but higher than the tritohydrate.

To identify the steps in SG11CC, isobaric PXRD in situ experiments were carried out once more. The anhydrate at the beginning and the end of the measurement, and the dihydrate at the lowest temperature, matched those in the pure salt, with an additional amorphous reflection similar to the SG in SG6CC. The mixed state of mono- and dihydrate during hydration, as observed in SG6CC, was also present in SG11CC, as depicted in Fig. 6a). However, also during dehydration, an intermediate step was detected, as suggested by the TGA curve. This dehydration intermediate also constituted a mixed state, comprising mono- and anhydrate, as illustrated in Fig. 6b). The most discernible reflections of the monohydrate were observed at 2θ around 15 and 35°, along with those of the anhydrate at 2θ approximately 19.5 and 43.5°. Since the SG11CC shows both this dehydration intermediate and more prominent monohydrate reflections compared to the dihydrate ones for the hydration intermediate, it is assumed that the pore size allows or hinders the formation of the monohydrate for the SG11CC and SG6CC, respectively.

The SG11CC composite, unlike the HCC composite, exhibited distinct hydration steps despite having a comparable average pore size (11 nm versus 15 nm). Notably, SG11CC showed no tritohydrate formation, whereas HCC clearly formed tritohydrate as evidenced by PXRD results and phase transition onsets. Comparison of SG11CC's phase transition onset with the phase diagram outlined in Ref. [43] revealed that its larger hydration and dehydration steps overlapped with SG6CC's onset, while smaller steps aligned with 1–2 onsets during hydration and 1-0 onset during dehydration.

The various composites - VCC, HCC, SCC, SG11CC, and SG6CC - demonstrate that tritohydrate formation is impeded in smaller pores compared to larger ones, as summarized in Fig. 7. In VCC, most of the salt hydrates through the tritohydrate phase, whereas in HCC, only about half does, and in the other composites, no tritohydrate is detected. Consequently, tritohydrate is observed in composites with an average pore diameter of 15 nm or more, while it remains undetectable in those with smaller pores.

It is possible that tritohydrate forms in smaller pores but in amounts too small to be detected by PXRD. The absence of detectable tritohydrate in these smaller pores underscores how pore size - and, consequently, the space available for $CaCl_2$ phase transitions affects hydration steps. In the case of SG composites, it also influences dehydration.

The preference for monohydrate over tritohydrate can be explained by comparing the unit cell volumes of the hydrates, as shown in Table 4. Generally, the unit cell volume increases with the amount of water in the crystal structure, from the anhydrate (0 mol H_2O/mol $CaCl_2$) to the dihydrate (2 mol H_2O/mol $CaCl_2$). However, an exception occurs with tritohydrate (1/3 mol H_2O/mol $CaCl_2$), which has the largest unit cell among the four hydrates examined in this study. By contrast, aside from the anhydrate, monohydrate has the smallest unit cell. This suggests that tritohydrate requires the formation of the largest nuclei among the hydrates, making its formation more challenging in confined spaces such as pores. The reason behind this larger nucleus is the requirement for a certain number of unit cells in each direction to be recognized as a

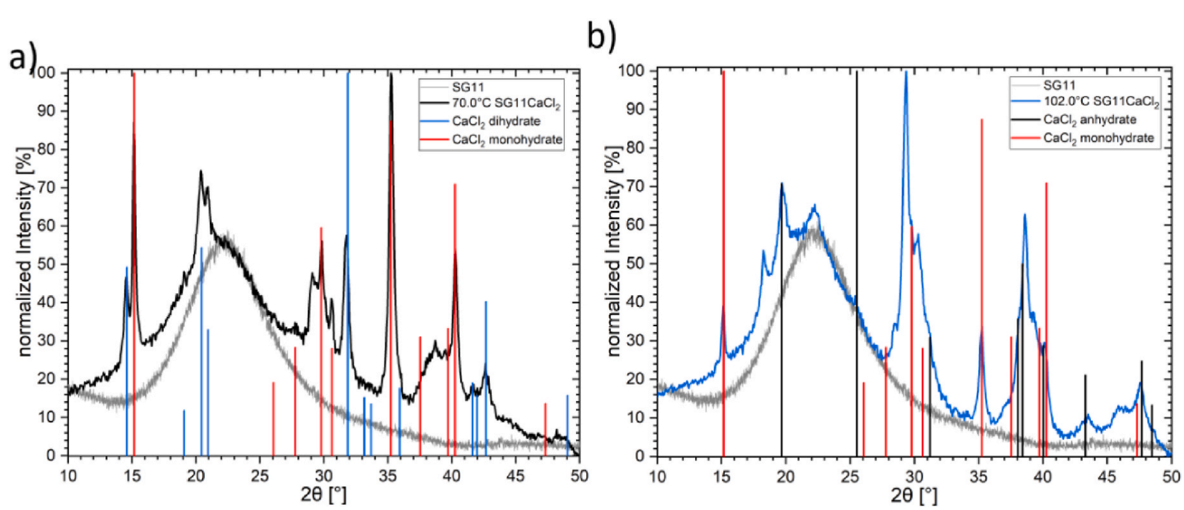

Fig. 6. The results from isobaric PXRD in-situ at 12 mbar from a) SG11+CaCl2 hydration, and b) SG11+CaCl2 dehydration.

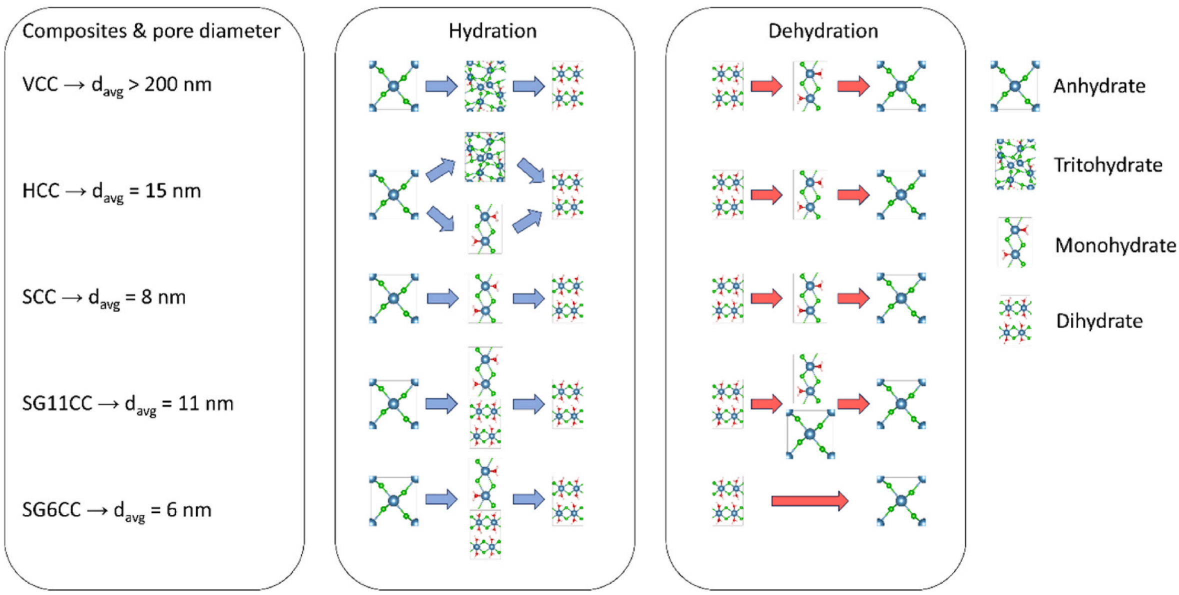

Fig. 7. The summary of the hydration and the dehydration steps observed in the different composites examined in this study.

Table 4
The unit cells of the $CaCl_2$ hydrates taken from Refs. [43,66–72].

hydrate	Space group	symmetry	V nm [3]	a [Å]	b [Å]	c [Å]
anhydrate	*Pnnm*	Orthorhombic	0.169	6.24	6.43	4.20
tritohydrate	*Pnma*	Orthorhombic	0.943	10.85	9.91	8.77
monohydrate	*Pmmn*	Orthorhombic	0.185	8.39	3.82	5.77
dihydrate	*Pbcn*	Orthorhombic	0.531	5.89	7.47	12.07
α-tetrahydrate	P-1	Triclinic	0.331	6.59	6.37	8.56
β-tetrahydrate	$P2_1/c$	Monoclinic	1.060	8.92	10.22	12.79
γ-tetrahydrate	$P2_1/c$	Monoclinic	0.391	6.14	7.67	8.90
hexahydrate	*P*321	Trigonal	0.212	7.88	7.88	3.95

crystalline and not amorphous material. In such restricted environments, the smaller unit cell of monohydrate may be favored, as it allows for the formation of stable nuclei capable of converting all the salt in a composite.

The three composites with the smallest pores - SCC and SGxCCs - exhibit different hydration and dehydration steps (0-1-2-1-0 versus 0-(1 + 2)-2-(1 + 0)-0 or 0-2-0), despite having comparable average pore diameters (8 nm for SCC and 11 or 6 nm for SGxCCs). Examining the TGA curves in Fig. 3, the clay composites in Fig. 3a) still display clear hydration and dehydration steps similar to those of pure salt, with only minor effects from matrix adsorption, such as slight slopes in plateaus and increased maximum loading/uptake. In contrast, the SG composites in Fig. 3b), particularly SG6CC, exhibit more sloped curves and smoother onsets. Additionally, the hysteresis between hydration and dehydration appears narrower compared to the clay composites, resembling the adsorption behavior of the pure matrix (see SI).

This observation suggests that not only does the salt influence the water uptake of the matrix, but the structure of the matrix pore walls also interacts with the salt's water absorption. Therefore, pore size alone does not fully explain the variation in $CaCl_2$ hydrate transitions, highlighting the interaction between the salt and the matrix as a likely contributing factor.

4. Conclusion

In this study, the hydration and dehydration pathways of $CaCl_2$ impregnated into five distinct porous matrices (Vermiculite (macroporous), Halloysite (mesoporous), Sepiolite (micro-meso-porous), and two mesoporous silica gels (with average pore diameters of 11 nm and 6 nm)) were explored through isobaric TGA cycles and PXRD in situ measurements while being.

It was found that for the composites with matrices with an average pore size smaller than 15 nm, no tritohydrate was detected as was the case for the pure $CaCl_2$ and composites with larger pores during hydration. This can be explained by the difference in unit cell volume between the two intermediate phases of the trito- and the monohydrate (see Table 4). The tritohydrate is hindered in its formation inside the limited space of the pore systems due to its large unit cell size and hence large nuclei, while the monohydrate has a very small unit cell size and thus nuclei, which are not hindered in their formation and growth.

Furthermore, in the silica gel composites, also the monohydrate step is nearly or completely skipped in favor of direct hydration from the anhydrate to the dihydrate and the reverse for the dehydration. The results display water uptake behavior that is strongly influenced by the type of matrix used rather than only the salt in the composite. Thus, not only does the salt affect the water uptake of a matrix in a composite but also the influence of the matrix adsorption on the salt absorption can be assumed.

The preference for the monohydrate over the tritohydrate (SCC) or the avoidance of any intermediate step (SGxCC) can make the application of $CaCl_2$ composites for heat batteries simpler since no path-dependent steps with different charging and discharging temperatures have to be accounted for. This also ensures that whether the material is fully or only partially hydrated or dehydrated, the output and charging temperatures remain the same. The findings in this work show a strong influence of the confinement of $CaCl_2$ on its hydration/dehydration pathway. Additionally, the chemistry of the porous matrix affects these pathways. As a consequence, it is necessary to characterize a particular $CaCl_2$-composite in order to understand the output characteristics of the battery.

CRediT authorship contribution statement

Michaela C. Eberbach: Writing – review & editing. **A.I. Shkatulov:** Paul Tinnemans, Formal analysis, Data curation. **H.P. Huinink:** Writing – original draft, Investigation, Formal analysis, Data curation. **H.R. Fischer:** Writing – review & editing. **O.C.G. Adan:** Writing – review & editing.

Disclaimer

During the preparation of this work the author(s) used ChatGPT in order to improve the readability of some sentences. After using this tool/service, the author(s) reviewed and edited the content as needed and take(s) full responsibility for the content of the publication.

Declaration of competing interest

The authors declare that they have no known competing financial interests or personal relationships that could have appeared to influence the work reported in this paper.

Acknowledgements

This publication is part of the project Mat4Heat with project number 739.017.014 of the research program Materials For Sustainability which is (partly) financed by the Dutch Research Council (NWO).

We want to thank Hans Dalderop and Martijn Kurvers for the technical support with the different machines and computers and Dr. Natalia Mazur's help in device training and setting up measurements. Also, a thank you to Dr. Leyla-Cann Sögütoglu for the help in understanding the MSZ of salt hydrates.

Appendix A. Supplementary data

Supplementary data to this article can be found online at https://doi.org/10.1016/j.micromeso.2025.113605.

Data availability

Data will be made available on request.

References

[1] J. Hansen, R. Ruedy, M. Sato, K. Lo, Global surface temperature change, Rev. Geophys. 48 (2010), https://doi.org/10.1029/2010RG000345.

[2] V. Masson-Delmotte, P. Zhai, A. Pirani, S.L. Connors, C. Péan, S. Berger, N. Caud, Y. Chen, L. Goldfarb, M.I. Gomis, M. Huang, K. Leitzell, E. Lonnoy, J.B.R. Matthews, T.K. Maycock, T. Waterfield, O. Yelekçi, R. Yu, B. Zhou and (eds.), Climate Change 2021: The Physical Science Basis. Contribution of Working Group I to the Sixth Assessment Report of the Intergovernmental Panel on Climate Change, Cambridge University Press, Cambridge, United Kingdom and New York, NY, USA, DOI: https://doi.org/10.1017/9781009157896.

[3] Summary for policymakers, in: H. Lee, J. Romero (Eds.), Climate Change 2023: Synthesis Report. Contribution of Working Groups I, II and III to the Sixth Assessment Report of the Intergovernmental Panel on Climate Change, IPCC, 2023, pp. 1–34, https://doi.org/10.59327/IPCC/AR6-9789291691647.001.

[4] Vaclav Smil, Energy Transitions: History, Requirements, Prospects, Praeger, 2010. ISBN: 978-0-313-38177-5.

[5] Hasila Jarimi, Devrim Aydin, Zhang Yanan, Gorkem Ozankaya, Xiangjie Chen, Saffa Riffat, Review on the recent progress of thermochemical materials and processes for solar thermal energy storage and industrial waste heat recovery, Oxford Academic - International Journal of Low-Carbon Technologies 14 (2018) 44–69, https://doi.org/10.1093/ijlct/cty052.

[6] D. Dicaire, F.H. Tezel, Regeneration and efficiency characterization of hybrid adsorbent for Thermal Energy Storage of excess and solar heat, Renew. Energy 36 (2010) 986–992, https://doi.org/10.1016/j.renene.2010.08.031.

[7] J. Jänchen, D. Ackermann, H. Stach, W. Brösicke, Studies of the water adsorption on zeolites and modified mesoporous materials for seasonal storage of solar heat, Sol. Energy 76 (2003) 339–344, https://doi.org/10.1016/j.solener.2003.07.036.

[8] L.C. Sögütoglu, P.A.J. Donkers, H.R. Fischer, H.P. Huinink, O.C.G. Adan, In-depth investigation of thermochemical performance in a heat battery: cyclic analysis of K_2CO_3, $MgCl_2$ and Na_2S, Appl. Energy 215 (2018) 159–173, https://doi.org/10.1016/j.apenergy.2018.01.083.

[9] P.A.J. Donkers, L.C. Sögütoglu, H.P. Huinink, H.R. Fischer, O.C.G. Adan, A review of salt hydrates for seasonal heat storage in domestic applications, Appl. Energy 199 (2017) 45–68, https://doi.org/10.1016/j.apenergy.2017.04.080.

[10] P. Tatsidjodoung, N. Le Pierrés, L. Luo, A review of potential materials for thermal energy storage in building applications, Renew. Sustain. Energy Rev. 18 (2012) 327–349, https://doi.org/10.1016/j.rser.2012.10.025.

[11] L. Scapino, H.A. Zondag, J. Van Bael, J. Diriken, C.C.M. Rindt, Sorption heat storage for long-term low-temperature applications: a review on the advancements at material and prototype scale, Appl. Energy 190 (2017) 920–948, https://doi.org/10.1016/j.apenergy.2016.12.148.

[12] K.E. N'Tsoukpoe, H. Liu, N. Le Pierrès, L. Luo, A review on long-term sorption solar energy storage, Renew. Sustain. Energy Rev. 13 (2009) 2385–2396, https://doi.org/10.1016/j.rser.2009.05.008.

[13] N. Yu, R.Z. Wang, L.W. Wang, Review - sorption thermal storage for solar energy, Prog. Energy Combust. Sci. 39 (2013) 489–514, https://doi.org/10.1016/j.pecs.2013.05.004.

[14] Ruby-Jean Clark, Abbas Mehrabadi, Mohammed Farid, State of the art on salt hydrate thermochemical energy storage systems for use in building applications, J. Energy Storage 27 (2020) 101145, https://doi.org/10.1016/j.est.2019.101145.

[15] Yu I. Aristov, Novel materials for adsorption heat pumping and storage: screening and nanotailoring of sorption properties, J. Chem. Eng. Jpn. 40 (2007) 1242–1251, https://doi.org/10.1252/jcej.07WE228.

[16] Ting Yan, Hong Zhang, A critical review of salt hydrates as thermochemical sorption heat storage materials: thermophysical properties and reaction kinetics, Sol. Energy 242 (2022) 157–183, https://doi.org/10.1016/j.solener.2022.07.002.

[17] Someshower Dutt Sharma, Hiroaki Kitano, Kazunobu Sagara, Phase change materials for low temperature solar thermal applications, Res. Rep. Fac. Eng. Meiji Univ. 29 (2004) 31–64.

[18] Miroslaw S. Gruszkiewicz, John M. Simonson, Vapor pressures and isopiestic molalities of concentrated $CaCl_2$(aq), $CaBr_2$(aq), and NaCl(aq) to T=523 K, J. Chem. Therm. 37 (2005) 906–930, https://doi.org/10.1016/j.jct.2004.12.009.

[19] F. Berroug, E.K. Lakhal, M. El Omari, M. Faraji, H. El Qarnia, Thermal performance of a greenhouse with a phase change material north wall, Energy Build. 43 (2011) 3027–3035, https://doi.org/10.1016/j.enbuild.2011.07.020.

[20] Kamil Kaygusuz, Experimental and theoretical investigation of latent heat storage for water based solar heating systems, Energy Convers. Manag. 36 (1995) 315–326, https://doi.org/10.1016/0196-8904(95)98896-U.

[21] Ahmed M. Hamed, Ahmed A. Sultan, Mass transfer in vertical cloth layers impregnated with calcium chloride for recovery of water from air, Renew. Energy 27 (2002) 13–25, https://doi.org/10.1016/S0960-1481(01)00176-8.

[22] Liu Hui, N'Tsoukpoe K. Edem, Le Pierres Nolwenn, Luo Lingai, Evaluation of a seasonal storage system of solar energy for house heating using different absorption couples, Energy Convers. Manag. 52 (2011) 2427–2436, https://doi.org/10.1016/j.enconman.2010.12.049.

[23] Ahmet Koca, Hakan F. Oztop, Tansel Koyun, Yasin Varol, Energy and exergy analysis of a latent heat storage system with phase change material for a solar collector, Renew. Energy 33 (2008) 567–574, https://doi.org/10.1016/j.renene.2007.03.012.

[24] S. Younus Ahmed, P. Gandhidasan, A.A. Al-Farayedhi, Thermodynamic analysis of liquid desiccants, Sol. Energy 62 (1998) 11–18, https://doi.org/10.1016/S0038-092X(97)00087-X.

[25] S. Hiebler, H. Mehling, M. Helm, C. Schweigler, Latent heat storage with melting temperature 29 C supporting a solar heating and cooling system, in: Proc. 11th Int. Conf. Therm. Energy Storage Effstock, 2009.

[26] Claus E. Weinell, Peter I. Jensen, Kim Dam-Johansen, Hans Livbjerg, Hydrogen chloride reaction with lime and limestone: kinetics and sorption capacity, Ind. Eng. Chem. Res. 31 (Nr. 1) (1992) 164–171.

[27] L.F. Cabeza, J. Illa, J. Roca, F. Badia, H. Mehling, S. Hiebler, F. Ziegler, Middle term immersion corrosion tests on metal-salt hydrate pairs used for latent heat storage in the 32 to 36°C temperature range, Materials and Corrosion/Werkstoffe und Korrosion 52 (2001) 748–754, https://doi.org/10.1002/1521-4176(200110)52:10<748::AID-MACO748>3.0.CO;2-S.

[28] V.V. Tyagi, D. Buddhi, Thermal cycle testing of calcium chloride hexahydrate as a possible PCM for latent heat storage, Sol. Energy Mater. Sol. Cell. 92 (2008) 891–899, https://doi.org/10.1016/j.solmat.2008.02.021.

[29] Gmelin-Institut für anorganische chemie und grensgebiete inder Max-Planck-Gesellschaft zur Förderung der Wissenschaft - Gmelins Handbuch der anorganischen Chemie - 8. Auflage - Calcium Teil B Lieferung 1-2, Verlag Chemie GmbH, Weinheim/Bergstrasse, J. Chem. Educ. 34 (1957), https://doi.org/10.1021/ed034p104.1.

[30] H.W. Bakhuis Roozeboom, Experimentelle und theoretische Studien über die Gleichgewichtsbedingungen zwischen festen und flüssigen Verbindungen von Wasser mit Salzen, besonders mit dem Chlorcalcium, Z. Phys. Chem. (1889), https://doi.org/10.1515/zpch-1889-0405.

[31] Henry Bassett, Geoffrey W. Barton, Albert R. Foster, Cyril R.J. Pateman, The ternary systems constituted by mercuric chloride, water, and an alkaline-earth chloride or cupric chloride, J. Chem. Soc. (1933) 151–164, https://doi.org/10.1039/JR9330000151.

[32] G.C. Sinke, E.H. Mossner, J.L. Curnutt, Enthalpies of solution and solubilities of calcium chloride and its lower hydrates, J. Chem. Therm. 17 (1985) 893–899, https://doi.org/10.1016/0021-9614(85)90083-7.

[33] Margarethe Molenda, Jana Stengler, Marc Linder, Antje Wörner, Reversible hydration behavior of $CaCl_2$ at high H_2O partial pressures for thermochemical energy storage, Thermochim. Acta 560 (2013) 76–81, https://doi.org/10.1016/j.tca.2013.03.020.

[34] Hiroshi Kimura, Junjiro Kai, Mixtures of calcium chloride hexahydrate with some salt hydrates or anhydrous salts as latent heat storage materials, Energy Convers. Manag. 28 (1988) 197–200, https://doi.org/10.1016/0196-8904(88)90021-0.

[35] Lichan Du, Jing Ding, Heqing Tian, Weilang Wang, Xiaolan Wei, Ming Song, Thermal properties and thermal stability of the ternary eutectic salt NaCl-$CaCl_2$-$MgCl_2$ used in high-temperature thermal energy storage process, Appl. Energy 204 (2017) 1225–1230, https://doi.org/10.1016/j.apenergy.2017.03.096.

[36] Alexandra Grekova, Marina Solovyeva, Anastasiia Cherpakova, Mikhail Tokarev, Composites based on $CaCl_2$-$CaBr_2$ salt system for adsorption applications: designing the optimal sorbent for gas drying and air conditioning, Separations 10

(9) (2023), https://doi.org/10.3390/separations10090473. https://www.mdpi.com/2297-8739/10/9/473,ISSN:2297-8739.
[37] Wei Xu, Yuanyuan Wang, Hang Xing, Jinqing Peng, Yimo Luo, Optimization of UiO-66/$CaCl_2$ composite material for thermal energy storage, Microporous Mesoporous Mater. 355 (2023) 112574, https://doi.org/10.1016/j.micromeso.2023.112574.
[38] Ruby-Jean Clark, Mohammed Farid, Chapter 11 - Salt Hydrate-Based Composite Materials for Thermochemical Energy Storage, Low-Grade Thermal Energy Harvesting, 2022, pp. 225–246, https://doi.org/10.1016/B978-0-12-823690-1.00003-4.
[39] Suboohi Shervani, Curtis Strong, F. Handan Tezel, Magnesium sulphate hybrids with silica gel and activated alumina for thermal energy storage, J. Clean. Prod. 371 (2022) 133262, https://doi.org/10.1016/j.jclepro.2022.133262.
[40] Axel Lannung, Dampfdruckmessungen ddes systems calciumchlorid-wasser, Z. Anorg. Allg. Chem. 228 (1936) 1–18, https://doi.org/10.1002/zaac.19362280102.
[41] L. Glasser, Thermodynamics of inorganic hydration and of humidity control, with an extensive database of salt hydrate pairs, J. Chem. Eng. Data 59 (2014) 526–530, https://doi.org/10.1021/je401077x.
[42] Hanane Ait Ousaleh, Said Sair, Said Mansouri, Younes Abboud, Mohamed Zahouily, Abdessamad Faik, Abdeslam El Bouari, Enhanced inorganic salts stability using bentonite clay for high-performance and low-cost thermochemical energy storage, J. Energy Storage 49 (2022) 104140, https://doi.org/10.1016/j.est.2022.104140.
[43] M.C. Eberbach, A.I. Shkatulov, P. Tinnemans, H.P. Huinink, H.R. Fischer, O.C. G. Adan, Path-dependent hydration and dehydration of $CaCl_2$, Cryst. Growth Des. (2025) [Manuscript submitted for publication].
[44] L.G. Gordeeva, Yu I. Aristov, Composites 'salt inside porous matrix' for adsorption heat transformation: a current state-of-the-art and new trends, Int. J. Low Carbon Technol. 7 (4) (2012) 288–302, https://doi.org/10.1093/ijlct/cts050,Eprint. ISSN: 1748-1317, https://academic.oup.com/ijlct/article-pdf/7/4/288/9644077/cts050.pdf.
[45] Dhammapada Mohapatra, Jalaiah Nandanavanam, Salt in matrix for thermochemical energy storage - a review, Mater. Today Proc. 72 (2023) 27–33, https://doi.org/10.1016/j.matpr.2022.05.453. ISSN: 2214-7853, https://www.sciencedirect.com/science/article/pii/S2214785322037737. International Conference on "Novel Materials and Technologies for Energy and Environment Applications.
[46] YuI. Aristov, M.M. Tokarev, G. Cacciola, G. Restuccia, Selective water sorbents for multiple applications, 1. $CaCl_2$ confined in mesopores of silica gel: sorption properties, React. Kinet. Mech. Catal. 59 (1996) 335–342.
[47] Yuri I. Aristov, Giovanni Restuccia, M.M. Tokarev, H.-D. Buerger, Angelo Freni, Selective water sorbents for multiple applications. 11. $CaCl_2$ confined to expanded vermiculite, React. Kinet. Catal. Lett. 71 (2000) 377–384, https://doi.org/10.1023/A:1010351815698.
[48] Marina V. Solovyeva, Irina V. Krivosheeva, Larisa G. Gordeeva, Alexander E. Khudozhitkov, Daniil I. Kolokolov, Alexander G. Stepanov, Ralf Ludwig, Salt confined in MIL-101(Cr)-Tailoring the composite sorbents for efficient atmospheric water harvesting, ChemSusChem 16 (2018) 1864–5631, https://doi.org/10.1002/cssc.202300520.
[49] Amira Jabbari-Hichri, Simona Bennici, Aline Auroux, $CaCl_2$-containing composites as thermochemical heat storage materials, Sol. Energy Mater. Sol. Cell. 172 (2017) 177–185, https://doi.org/10.1016/j.solmat.2017.07.037. ISSN: 0927-0248, https://www.sciencedirect.com/science/article/pii/S0927024817304300.
[50] Sean P. Casey, Jon Elvins, Saffa Riffat and Andrew Robinson, Salt impregnated desiccant matrices for 'open' thermochemical energy storage—selection, synthesis and characterisation of candidate materials, Energy Build. 84 (2014) 412–425, https://doi.org/10.1016/j.enbuild.2014.08.028.
[51] Yanan Zhang, Ziwei Chen, Cagri Kutlu, Yuehong Su, Saffa Riffat, Investigation on a vermiculite-based solar thermochemical heat storage system for building applications, Future Cities and Environment 8 (2022) 8, https://doi.org/10.5334/fce.153.
[52] M. Gaeini, A.L. Rouws, J.W.O. Salari, H.A. Zondag, C.C.M. Rindt, Characterization of microencapsulated and impregnated porous host materials based on calcium chloride for thermochemical energy storage, Appl. Energy 212 (2018) 1165–1177, https://doi.org/10.1016/j.apenergy.2017.12.131.
[53] Siyu Wei, Wei Zhou, Rui Han, Jihui Gao, Guangbo Zhao, Yukun Qin, Chunhao Wang, Influence of minerals with different porous structures on thermochemical heat storage performance of $CaCl_2$-based composite sorbents, Sol. Energy Mater. Sol. Cell. 243 (2022) 111769, https://doi.org/10.1016/j.solmat.2022.111769.
[54] Elise Bérut, Laurence Bois, Quentin Touloumet, Jonathan Outin, Michel Ondarts, Georgeta Postole, María José Rueda López, Aline Auroux, Nolwenn Le Pierrès, Characterization of silica-PEG-$CaCl_2$ composite sorbents in an open thermochemical heat storage reactor, J. Energy Storage 72 (2023) 108632, https://doi.org/10.1016/j.est.2023.108632.
[55] M.C. Eberbach, H.P. Huinink, A.I. Shkatulov, H.R. Fischer, O.C.G. Adan, The effect of nanoconfinement on deliquescence of $CuCl_2$ is stronger than on hydration, Cryst. Growth Des. 23 (2023) 1343–1354, https://doi.org/10.1021/acs.cgd.2c00821.
[56] Yu I. Aristov, Novel materials for adsorption heat pumping and storage: screening and nanotailoring of sorption properties, J. Chem. Eng. Jpn. 40 (2007) 1242–1251, https://doi.org/10.1252/jcej.07WE228.
[57] Emilie Courbon, Pierre D'Ans, Anastasia Permyakova, Oleksandr Skrylnyk, Nathalie Steunou, Marc Degrez, Marc Frère, A new composite sorbent based on $SrBr_2$ and silica gel for solar energy storage application with high energy storage density and stability, Appl. Energy 190 (2017) 1184–1194.
[58] Gareth Whiting, Didier Grondin, Simona Bennici, Aline Auroux, Heats of water sorption studies on zeolite-$MgSO_4$ composites as potential thermochemical heat storage materials, Sol. Energy Mater. Sol. Cells 112 (2013) 112–119.
[59] Gareth T. Whiting, Didier Grondin, Dusan Stosic, Simona Bennici, Aline Auroux, Zeolite-$MgCl_2$ composites as potential long-term heat storage materials: influence of zeolite properties on heats of water sorption, Sol. Energy Mater. Sol. Cells 128 (2014) 289–295.
[60] E.P. Barrett, L.G. Joyner, P.P. Halenda, The determination of pore volume and area distributions in porous substances. I. Computations from nitrogen isotherms, J. Am. Chem. Soc. 73 (1951) 373–380, https://doi.org/10.1021/ja01145a126.
[61] S. Brunauer, P.H. Emmett, E. Teller, Adsorption of gases in multimolecular layers, J. Am. Chem. Soc. 60 (1938) 309–319, https://doi.org/10.1021/ja01269a023.
[62] P. Gabbott, Principles and Applications of Thermal Analysis, John Wiley & Sons, 2008, https://doi.org/10.1002/9780470697702. ISBN: Print: 9781405131711, Online: 9780470697702.
[63] Greenspan Lewis, Humidity fixed points of binary saturated aqueous solutions, Journal of Research of the National Bureau of Standards - A. Physics and Chemistry 81 (A) (1977) 89–96, https://doi.org/10.6028/jres.081A.011.
[64] Leyla-Cann Sögütoglu, Fundamentals of Salt Hydration for Heat Battery Application, Eindhoven University of Technology, 2020. ISBN: 978-90-386-5063-0, https://research.tue.nl/en/publications/fundamentals-of-salt-hydration-for-heat-battery-application. (Accessed 7 September 2022).
[65] Leyla-Cann Sögütoglu, Michael Steiger, Jelle Houben, Daan Biemans, Hartmut R. Fischer, Pim Donkers, Henk Huinink, Olaf C.G. Adan, Understanding the hydration process of salts: the impact of a nucleation barrier, Cryst. Growth Des. 19 (2019) 2279–2288, https://doi.org/10.1021/acs.cgd.8b01908.
[66] A.K. van Bever, W. Nieuwenkamp, Die Kristallstruktur von Calciumchlorid, $CaCl_2$, Zeitschrift für Kristallographie, Kristallgeometrie, Kristallphysik, Kristallchemie 90 (1935) 374–376, https://doi.org/10.1524/ZKRI.1935.90.1.374. COD-code: 1011280, AMS-code: 0018132.
[67] R.W.G. Wyckoff, Crystal Structures, second ed., vol. 1, 1963, pp. 239–444, https://doi.org/10.1107/S0365110X65000361. COD-code: 9009084, AMS-code: 0011763.
[68] A. Leclair, M.M. Borel, Le dichlorure de calcium dihydrate, Acta Crystallogr. B 33 (1977) 1608–1610, https://doi.org/10.1107/S0567740877006645. COD-code: 1001835, AMS-code: 0009590.
[69] A. Leclaire, M.M. Borel, Liaisons hydrogène et coordination du calcium dans les cristaux de $CaCl_2 \cdot 4H_2O\alpha$, Acta Crystallogr. B 35 (1979) 585–588, https://doi.org/10.1107/S0567740879004209. COD-code: 9015889.
[70] A. Leclaire, M.M. Borel, La forme β du dichlorure de calcium tetrahydrate, Acta Crystallogr. B 34 (1978) 900–902, https://doi.org/10.1107/S0567740878004288. COD-code: 1001018.
[71] A. Leclaire, M.M. Borel, J.C. Monier, La forme γ du dichlorure de calcium tetrahydrate, Acta Crystallogr. B 36 (1980) 2757–2759, https://doi.org/10.1107/S0567740880009909. COD-code: 1001110.
[72] A. Leclaire, M.M. Borel, Le dichlorure et le dibromure de calcium hexahydratés, Acta Crystallogr. B 33 (1977) 2938–2940, https://doi.org/10.1107/S0567740877009881. COD-code: 1001770.